JACS
JOURNAL OF THE AMERICAN CHEMICAL SOCIETY
Article
pubs.acs.org/JACS

3-Helix Micelles Stabilized by Polymer Springs

He Dong,[†] Jessica Y. Shu,[†] Nikhil Dube,[†] Yufei Ma,[†] Matthew V. Tirrell,[‡,⊥] Kenneth H. Downing,[∥] and Ting Xu*[,†,⊥,§]

[†]Department of Materials Science and Engineering, [‡]Department of Bioengineering, and [§]Department of Chemistry, University of California - Berkeley, Berkeley, California, United States

[⊥]Materials Sciences Division, and [∥]Life Sciences Division, Lawrence Berkeley National Laboratory, Berkeley, California, United States

Supporting Information

ABSTRACT: Despite increasing demands to employ amphiphilic micelles as nanocarriers and nanoreactors, it remains a significant challenge to simultaneously reduce the particle size and enhance the particle stability. Complementary to covalent chemical bonding and attractive intermolecular interactions, entropic repulsion can be incorporated by rational design in the headgroup of an amphiphile to generate small micelles with enhanced stability. A new family of amphiphilic peptide−polymer conjugates is presented where the hydrophilic headgroup is composed of a 3-helix coiled coil with poly(ethylene glycol) attached to the exterior of the helix bundle. When micelles form, the PEG chains are confined in close proximity and are compressed to act as a spring to generate lateral pressure. The formation of 3-helix bundles determines the location and the directionalities of the force vector of each PEG elastic spring so as to slow down amphiphile desorption. Since each component of the amphiphile can be readily tailored, these micelles provide numerous opportunities to meet current demands for organic nanocarriers with tunable stability in life science and energy science. Furthermore, present studies open new avenues to use energy arising from entropic polymer chain deformation to self-assemble energetically stable, single nanoscopic objects, much like repulsion that stabilizes bulk assemblies of colloidal particles.

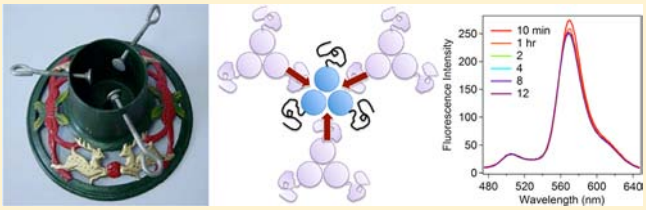

INTRODUCTION

Amphiphilic molecules can spontaneously self-assemble into micelles and have been routinely used to generate multifunctional nanocarriers with different particle size, shape, composition, and internal structures.[1−9] Micelles less than 20 nm in size with tunable stability and controlled time scales of disassembly will have significant impact in nanomedicine,[3,10,11] nanoreactors and catalysis,[12,13] and nanocrystal−micelle arrays,[14] etc. but yet remain a significant challenge. Thermodynamically, micelle formation reflects a balance between interfacial interactions between the surface and the local medium and the cohesive energy stored in the micelle. The thermodynamic stability of a micelle is inversely proportional to the critical micelle concentration (CMC) and can be tailored by adjusting the length and hydrophobicity of the hydrophobic tail to improve micelle stability upon dilution. The most extensively studied amphiphiles are small-molecule surfactants and amphiphilic block copolymers (BCPs) that exhibit a wide range of CMCs ranging from nanomolar to millimolar.[15−18]

Different from other organic nanoparticles stabilized by covalent bonds such as dendrimers,[19−21] micelles are dynamic, fluidic assemblies where individual amphiphiles (called "unimers") constantly exchange with the medium and with other micelles. The rate of subunit exchange determines the kinetic stability of a micelle and can be accelerated with continuous removal of unimers. Although stable polymeric micelles with hydrodynamic diameters of 50−150 nm have been recently reported,[22−24] micelles between 10 and 20 nm in size generally are not as stable, exhibiting typical exchange half-lives of a few hours.[25,26] This dramatically compromises their potential as nanocarriers or nanoreactors. Subunit exchange is a two-step process where a unimer desorbs from a micelle, followed by rapid insertion into another micelle.[27,28] Unimer desorption is the rate-limiting step, and its activation energy barrier depends on the length of the hydrophobic block and the intermolecular interactions and steric hindrance between each component of both the head and the tail block.[29−33] Increasing the hydrophobic chain length beyond certain values may lead to kinetically trapped heterogeneous aggregates. Chemically cross-linking the headgroups effectively reduces the unimer desorption kinetics and stabilizes the micelle.[34,35] Specific chemical degradation of covalent bonds can be engineered to disassemble micelles as needed.[36,37] Alternatively, engineering multiple pairs of intermolecular interactions, typically a few kilocalories per mole, among the headgroups can also increase the activation energy barrier for desorption.[38] The presence of competing interactions in the surrounding environment also affects subunit exchange kinetics. Repulsive interactions between closely positioned objects are entropic in nature and are not subject to competing attractive interactions.[39] The

Received: May 17, 2012
Published: June 25, 2012

   dx.doi.org/10.1021/ja3048128 | J. Am. Chem. Soc. 2012, 134, 11807−11814

chemical potential increases rapidly with decreasing separation distance and can reach tens of kilocalories per mole, comparable to energies stored in covalent bonds.[39−41] The interplay of repulsive and attractive interactions among viral capsid proteins has led to the formation of viruses with uniform structure and controlled stability.[42−44] Rational design to incorporate intermolecular interactions and entropic repulsion in the headgroup of an amphiphile may potentially overcome current bottlenecks to generate small micelles with tunable stability.

We recently reported a new family of amphiphilic peptide−polymer conjugates based on a common protein tertiary structure, 3-helix bundle, that form spherical micelles with 15 nm diameter.[11] Despite the small size of these micelles, they exhibited a long blood circulation half-life of 29 h, comparable to some of the successful dendrimers.[21,45] In order to further understand the structure and stability of these micelles, the current study is focused on elucidating a range of parameters governing the kinetic stability. Figure 1a shows the design of an amphiphile based on a 3-helix peptide−polymer conjugate. It consists of a short peptide helix with a poly(ethylene glycol) (PEG) chain covalently attached to the middle of the helix and two hydrophobic tails (C16) attached to the N-terminus. The peptides self-associate into 3-helix bundles, forming a trimeric subunit where three PEG chains are anchored to the exterior of 3-helix bundles, as schematically shown in the top view and side view in Figure 1a. Figure 1b shows a picture of a Christmas tree stand where three screws hold the tree in place. The screws are positioned so that the force vectors applied are balanced to prevent the tree from being pulled out in the vertical direction. We extrapolate the strategy to be applied to tailor the desorption kinetics of amphiphile unimers and, consequently, the kinetic stability of small micelles. When micelles form, the PEG chains are confined in close proximity and are compressed in comparison to its solution conformation. Solution small-angle X-ray scattering on the headgroup showed that, when the PEG chains are conjugated in the middle of the peptide chain, they are slightly compressed with a radius of gyration of ∼1.2 nm.[46] Thus, the PEG chains act as elastic springs and exert repulsive forces to push the neighboring amphiphilic subunit. The formation of 3-helix bundles determines the location and the directionalities of the force vector of each PEG elastic spring so as to slow down amphiphile desorption, similar to the design used in the Christmas tree stand.

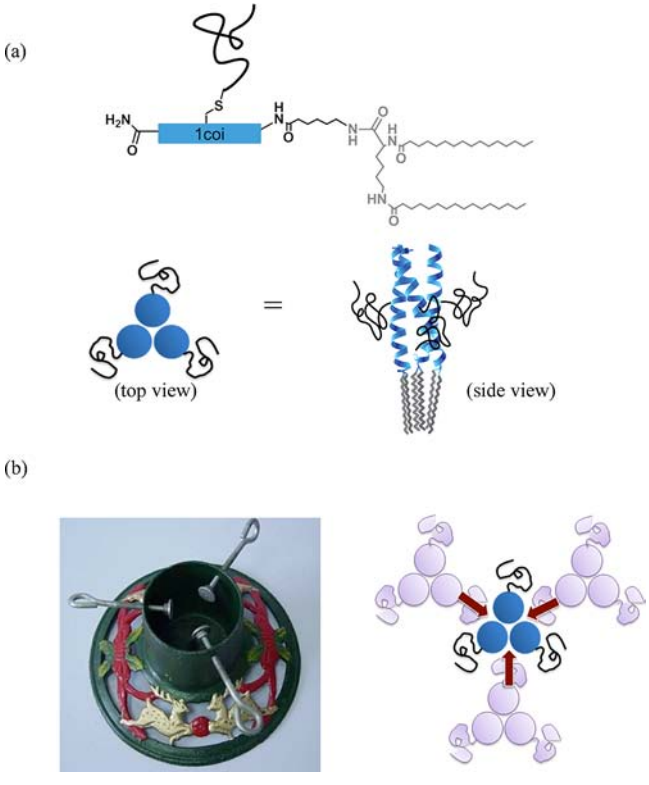

Figure 1. (a) Chemical structure of the monomeric subunit composed of the peptide (1coi), double C16 tails (gray), and PEG chains (black). Schematic drawing of the designed amphiphilic trimeric subunit where the headgroup contains a 3-helix bundle with the polymer covalently attached to the exterior. When micelles form, the PEG chains are confined in close proximity and are compressed in comparison to their solution conformation. (b) Picture of Christmas tree stand where three screws push in to hold the tree in place. The same design principle was utilized to stabilize the 3-helix micelle by means of entropic repulsion.

EXPERIMENTAL METHODS

Synthesis of Amphiphilic Peptide−Polymer Conjugates and Fluorescein-Labeled Peptide−Polymer Conjugates. PDB 1coi (EVEALEKKVAALECKVQALEKKVEALEHGW), SingleHelix (EAEAAEKKAAAAECKAQAAEKKAEAAEHGW), Scmb (EGKAGEKAGAALKCGVQELEKGAEAGEGGW) were synthesized using solid phase peptide synthesis (SPPS). For the synthesis of amphiphilic subunits, the alkyl chains were conjugated through reaction of palmitic acids with deprotected Fmoc-Lys(Fmoc)-OH to generate a branched alkyl tail at the N-terminus. Modification of the C-terminus was achieved through orthogonal protection strategy employed in Fmoc-SPPS. Specifically, the alloc group on the lysine residue at the C-terminus was selectively removed by utilizing $Pd(PPh_3)_4$ catalyst and a radical trapping agent, $PhSiH_3$ in DCM. The reaction was repeated five times. The resulting free amino groups of lysine were utilized for conjugating carboxy-terminated fluorescein using HBTU/DIPEA chemistry. The coupling reaction was performed at room temperature for 24 h and repeated twice. Cleavage was carried out using a cocktail of 90:8:2 TFA/TIS/water for 3 h. Crude peptides were precipitated in cold ether, isolated, and dried for the conjugation of polymers. To conjugate PEG, cysteine at position 14 facilitates the site-specific coupling of maleimide-functionalized PEG of molecular weight 2000 g/mol to the middle of the peptide sequence. The conjugation reaction was carried out in phosphate buffer (pH = 6.2) overnight with a reaction ratio of PEG to peptide at 5:1.

Small-Angle X-ray Scattering (SAXS). SAXS was carried out at beamline 7.3.3 at the Advanced Light Source, Lawrence Berkeley National Laboratory. Samples were dissolved in 25 mM KH_2PO_4, pH 7.4 buffer at a range of concentrations, from 0.5 to 16 wt %. Samples of the lowest concentration were measured in a homemade circulating flow cell with 0.025 mm thick muscovite mica windows and counted 50 times for 5 s each time to garner the form factor. Samples of higher concentration were measured in 2 mm boron-rich thin-walled capillary tubes to investigate both the form and structure factors. Form factors were fit using the core−shell sphere model included in the SANS software analysis package provided by National Center for Neutron Research at National Institute of Standards and Technology (NCNR-NIST).

Cryo-TEM. Cryo sample preparation was done on a Vitrobot (FP5350/60). Five microliters of peptide solution was pipetted onto a holey carbon grid and blotted for 2 s to remove excess solution. The sample was quickly plunged into liquid ethane and transferred to a cryo holder containing liquid nitrogen. Samples were imaged on a JEOL 4000 microscope at −177 °C using low dose conditions.

Negatively Stained TEM. Lyophilized peptide powder was dissolved at 1 mg/mL in 25 mM phosphate buffer at pH 7.4. Five microliters of peptide solution was dropped on a discharged holey

carbon-coated grid (Ted Pella 01824). After removing excess peptide solution, 5 μL of phosphotungstic acid (2 wt %, pH = 3.3) solution was then applied for 2 min. Samples were dried in air and examined by a FEI Tecnai 12 transmission electron microscope at 120 kV.

Stability of Hybrid Micelles. A lipophilic FRET pair, 3,3′-dioctadecyloxacarbocyanine perchlorate (DiO, donor) and 1,1′-dioctadecyl-3,3,3′,3′-tetramethylindocarbocyanine perchlorate (DiI, acceptor) were used to measure the energy transfer upon dilution in bovine serum albumin (BSA). Desired amount of DiO, DiI, and 1coi–dC16–PEG2K or Scmb–dC16–PEG2K were codissolved in a mixture of 1:1 chloroform and methanol. Organic solvents were evaporated under vacuum at 60 °C for at least 3 h to form a thin film in a glass vial. Phosphate buffer (pH = 7.4, 25 mM) was added to rehydrate the film at a concentration of 1 mg/mL. In cases where visible aggregates were formed, the solution was heated in water bath at 70 °C for at least 30 min to promote the homogeneity of the encapsulation. After 24 h stirring at room temperature, the solutions were then subjected to centrifugation and spin dialysis to remove any insoluble aggregates and soluble dyes in the supernatant. 10 μL of the dye-containing micelle solution was mixed with 350 μL of BSA, and time-dependent fluorescence intensity was recorded in the range of 475–650 nm for 12 h with excitation wavelength at 450 nm.

RESULTS AND DISCUSSION

The amphiphiles were synthesized by covalently linking maleimide-functionalized PEG of 2000 Da to the Cys14 of a 3-helix bundle-forming peptide (Protein Data Bank code "1coi").[47,48] Two C16 alkyl chains were attached to the peptide N-terminus with a (6)-amino-hexanoic acid linker inserted between the peptide and the double alkyl tail. The resulting amphiphiles are called "1coi–dC16–PEG2K". 1coi–dC16–PEG2K forms uniform micelles, ~15 nm in diameter, spontaneously over a wide range of amphiphile concentrations above the CMC (4 μM) by simply dissolving the lyophilized amphiphile in aqueous media (Figure S1, Supporting Information [SI]). Panels a and b of Figure 2 show the cryo-TEM image and the TEM image of negatively stained dried nanoparticles, where micellar nanoparticles can be clearly seen. Solution small-angle X-ray scattering (SAXS) experiments (Figure 2c) indicate that the C16 alkyl tails form the hydrophobic core, ~5.6 nm in diameter, and the 1coi–PEG2K conjugates form the hydrophilic shell, ~4.6 nm in thickness.

Solutions of 1coi–dC16–PEG2K micelle exhibit exceptional stability against long-term storage even at high amphiphile concentrations. Figure 2d shows a series of SAXS profiles of 1coi–dC16–PEG2K solutions with concentrations ranging from 0.5 to 16 wt %. Scattering profiles at $q < 0.08$ Å^{-1} can be fit to a spherical core–shell model, similar to that shown in Figure 2c, confirming the integrity of individual micelles and the absence of random aggregates. As the volume fraction of micelles increases to 34 vol % at 16 wt % of 1coi–dC16–PEG2K, the micelles start to coassemble into structures with liquidlike ordering reflected by the broad diffraction peak at $q \approx 0.035$ Å^{-1} that corresponds to interparticle distances of ~18 nm. The micelles also exhibit exceptional long-term stability at room temperature with no storage requirements; the SAXS profile of a micelle solution remained the same after storage for 2 months at room temperature (Figure S2 in SI) and TEM (Figure S3 in SI) reveals micelle integrity after 9 months. In contrast, conjugate without PEG chain rapidly precipitated in phosphate buffer, leading to irregular aggregates. (Figure S4 in SI)

The stability of 1coi–dC16–PEG2K was further confirmed using the Förster resonance energy transfer (FRET) method. A lipophilic FRET pair, 3,3′-dioctadecyloxacarbocyanine perchlorate (DiO, donor) and 1,1′-dioctadecyl-3,3,3′,3′-tetramethylindocarbocyanine perchlorate (DiI, acceptor), were independently encapsulated in two batches of 1coi–dC16–PEG2K micelles. Upon mixing at room temperature, minimal fluorescence due to energy transfer was detected, and essentially no cargo leakage was observed after more than 44 h, showing an exceptional stability and inferring slow subunit exchange kinetics (Figure 3).

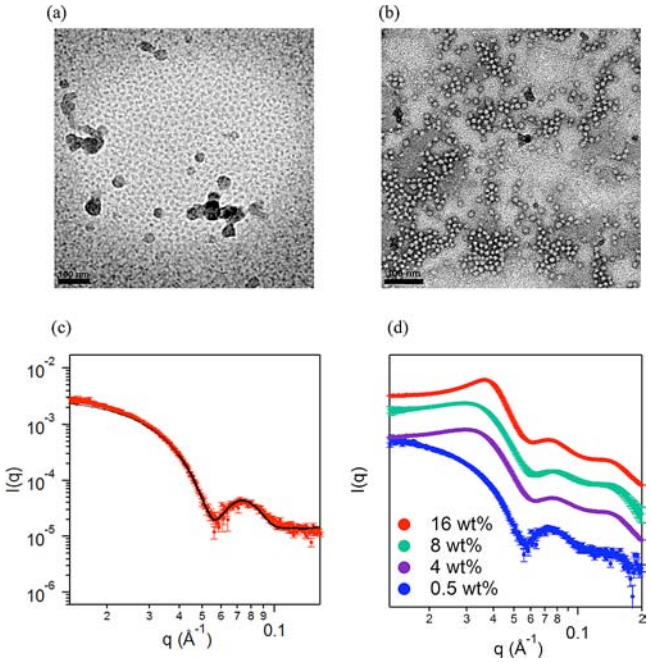

Figure 2. (a) Vitreous ice cryogenic TEM of 1coi–dC16–PEG2K at 1 mg/mL in 25 mM phosphate buffer at pH 7.4; (b) negatively stained TEM of 1coi–dC16–PEG2K at 1 mg/mL in 25 mM phosphate buffer at pH 7.4; (c) SAXS of 1coi–dC16–PEG2K at 5 mg/mL in 25 mM phosphate buffer. Fitting of the data (solid line) to a core–shell spherical form factor yields a core diameter of ~5.6 nm, a shell thickness of ~4.6 nm, and polydispersity of ~7%. (d) Concentration-dependent SAXS of 1coi–dC16–PEG2K in 25 mM phosphate buffer. Scattering profiles at scattering vector $q < 0.08$ Å^{-1} can be fitted using the micelle form factor for all samples studied.

The kinetics of subunit exchange of micelles was quantified by monitoring the fluorescence recovery of a self-quenching fluorophore, fluorescein, which was attached to the peptide C-terminus.[25,26] The conjugation of fluorescein was found not to interfere with micelle formation. Self-quenched fluorescently labeled micelles were mixed with a large excess of nonlabeled micelles. Subunit exchange between labeled micelles and nonlabeled micelles led to an increase in fluorescence intensity upon the addition of nonlabeled micelles. The relative fluorescence intensity change as a function of time is indicative of the rate of exchange kinetics. Figure 4 shows the fitting of the fluorescence recovery data into eq 1 with two first-order disassociation rate constants.

$$I(t) = I(\infty) + [I(0) - I(\infty)][f\mathbf{e}^{-k_1 t} + (1-f)\mathbf{e}^{-k_2 t}] \quad (1)$$

The fast rate constant, k_1 is attributed to the dilution of labeled micelles upon the addition of nonlabeled micelles, leading to an equilibrium shift toward fluorescently labeled unimers. The slower rate constant, k_2 represents the rate of monomer

dx.doi.org/10.1021/ja3048128 | J. Am. Chem. Soc. 2012, 134, 11807–11814

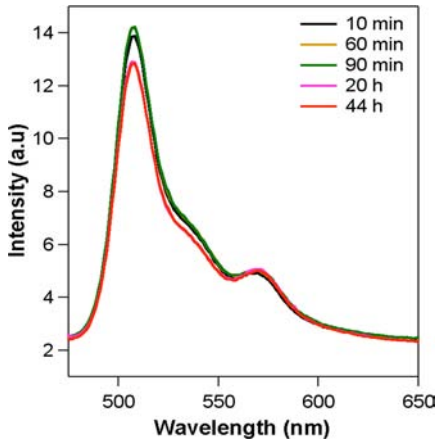

Figure 3. FRET spectra of a mixture of 1coi−dC16−PEG2K micelles encapsulating DiO and DiI FRET pair dyes. After 44 h, minimal fluorescence change due to energy transfer was observed, indicating the absence of cargo leakage. The excitation wavelength is 450 nm, and the emission spectrum was collected between 475 and 650 nm.

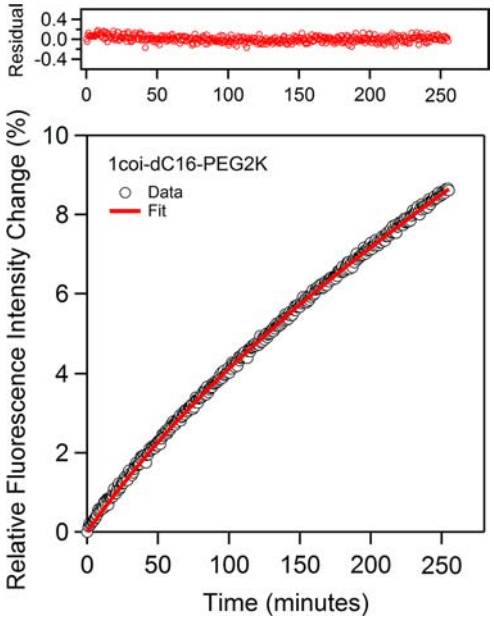

Figure 4. Fitting of fluorescence recovery data into first-order exchange kinetics. [labeled peptide] = 15 μM; [nonlabeled peptide] = 600 μM. Data were fitted into equation $I(t) = I(\infty) + [I(0) - I(\infty)][fe^{-k_1 t} + (1 - f)e^{-k_2 t}]$. The fast rate constant, k_1 is attributed to the dilution of the labeled micelles upon the addition of the nonlabeled micelles, leading to an equilibrium shift toward fluorescently labeled unimers. The slower rate constant, k_2 represents the rate of monomer desorption from labeled micelles followed by rapid incorporation into the nonlabeled micelles and can be used to compare the kinetics stability of different micelles.

desorption from labeled micelles followed by rapid incorporation into the nonlabeled micelles and can be used to compare the kinetics stability of different micelles. The fitting of fluorescence recovery data suggests very slow exchange kinetics with a first-order rate constant of 2.1×10^{-4} min^{-1}, corresponding to a half-life of 55 h. This is well within the time regime required for many applications of micellar nanoparticles in nanomedicine and nanoreactors.

Extensive studies have shown that the activation energy barrier for subunit desorption depends on the length of the hydrophobic block, the molecular weight of the desorbed amphiphile, and intermolecular interactions within the head and tail groups.[29,31,32,49] For the designed 3-helix bundle amphiphile, the protein structure of the headgroup affects the alkyl packing in the hydrophobic core, the molecular weight of desorbed amphiphiles, and the location and the chain conformation of the PEG chain. To decouple the effects of these parameters on micelle stability, two amphiphile analogues were synthesized where the headgroup was designed to form a single helix or a random coil, respectively. In the sequence, called "SingleHelix", the valine and leucine residues at the "a" and "d" positions in the heptad were mutated with alanine to disrupt the hydrophobic packing in the interior of the helix bundle and destabilize the 3-helix bundle formation. The circular dichroism (CD) spectrum (Figure 5) shows that the

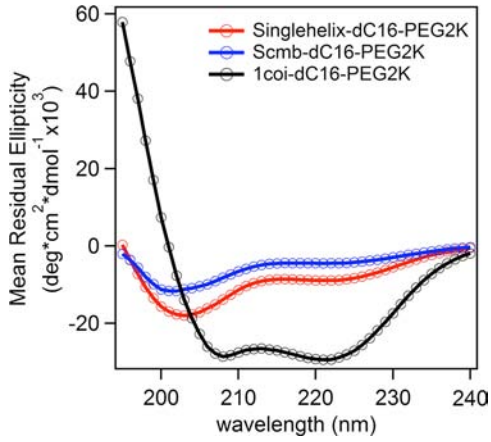

Figure 5. CD spectra of amphiphilic peptide−polymer conjugates with different headgroups. Peptide concentration: 200 μM. 1coi−dC16−PEG2K forms a coiled-coil α-helix. SingleHelix−dC16−PEG2K and Scmb−dC16−PEG2K form a mixed α-helix and random coil with 34% and 20% helicity, respectively.

SingleHelix-based amphiphile maintains the α-helical character with a helicity of 34%. The ratio of the mean residual ellipticity between 222 and 208 nm is 0.83, suggesting the absence of helix bundle formation. Another peptide, "Scmb", was designed to form a random coil structure by substituting hydrophobic residues at the "a" and "d" positions with glycine, and the helicity of the Scmb-based amphiphile is reduced to 20% at 20 °C. SingleHelix−dC16−PEG2K and Scmb−dC16−PEG2K form spherical micelles in aqueous solution, as shown by negatively stained TEM (Figure S5, SI) and size exclusion chromatography (SEC) (Figure S6, SI). Using the same pyrene encapsulation method, the CMC of SingleHelix−dC16−PEG2K and Scmb−dC16−PEG2K was determined to be ~4 μM (Figure S7, SI), suggesting the thermodynamic stability is comparable to that of 1coi−dC16−PEG2K micelle.

Fluorescence recovery experiments were carried out to evaluate the kinetics of subunit exchange of SingleHelix−dC16−PEG2K and Scmb−dC16−PEG2K micelles under the same condition as that of 1coi−dC16−PEG2K, as shown in Figure 4. For Scmb−dC16−PEG2K, a significant enhancement of fluorescence intensity (>140%) was observed over a 4-h period at 20 °C, and the subunit dissociation occurs with a first-order rate constant of 8.75×10^{-3} min^{-1}, corresponding to a half-life of 1.3 h (Figure 6a). Singlehelix−dC16−PEG2K showed an even faster subunit exchange kinetics and subunit desorption rate with a dissociation half-life of 0.9 h (Figure 6b).

dx.doi.org/10.1021/ja3048128 | J. Am. Chem. Soc. 2012, 134, 11807−11814

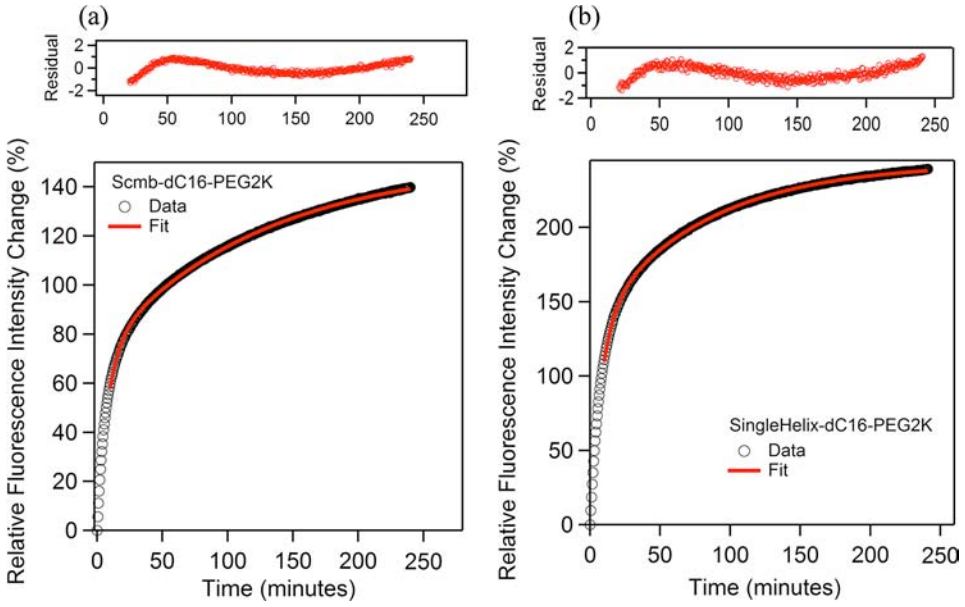

Figure 6. Fitting of fluorescence recovery data into first-order exchange kinetics. (a) Scmb−dC16−PEG2K. (b) SingleHelix−dC16−PEG2K. [labeled peptide] = 15 μM; [nonlabeled peptide] = 600 μM. Data were fitted into equation $I(t) = I(\infty) + [I(0) - I(\infty)][fe^{-k_1 t} + (1 - f)e^{-k_2 t}]$. The fast rate constant, k_1 is attributed to the dilution of labeled micelles upon the addition of nonlabeled micelles, leading to an equilibrium shift toward fluorescently labeled unimers. The slower rate constant, k_2 represents the rate of monomer desorption from labeled micelles followed by rapid incorporation into the nonlabeled micelles and can be used to compare the kinetics stability of different micelles. Thus, for Scmb−dC16−PEG2K and SingleHelix−dC16−PEG2K, data acquired after 20 min were chosen to be fitted into the equation as the new equilibrium is reached.

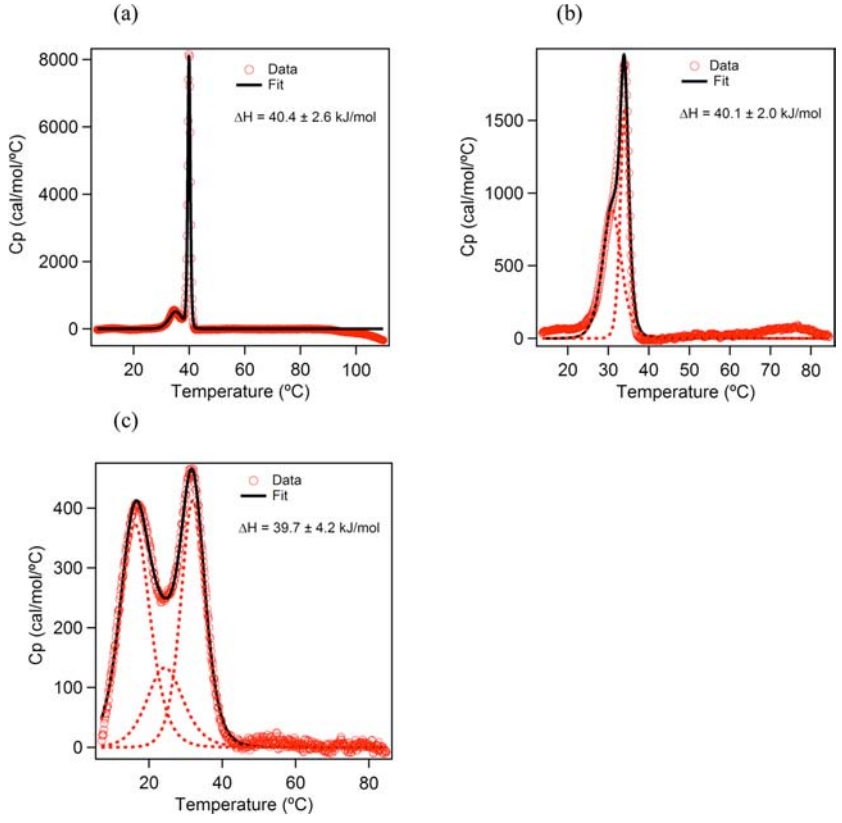

Figure 7. DSC thermograms of (a) Scmb−dC16−PEG2K (b) SingleHelix−dC16−PEG2K (c) 1coi−dC16−PEG2K. Sample concentration: 200 μM in phosphate buffer (25 mM, pH = 7.4). The endothermic peaks result from aliphatic chain melting in the hydrophobic core. The difference in melting temperatures observed indicates the effect of headgroup protein secondary and tertiary structure on the hydrophobic core packing.

In comparison, only an 8% increase in the fluorescence intensity was observed for 3-helix micelles composed of 1coi−dC16−PEG2K, and the micelle has a half-life of 55 h under the same experimental conditions. Comparing the recovery profile of the three amphiphiles with different protein structures in the headgroup, we conclude that the 3-helix bundle formation is

dx.doi.org/10.1021/ja3048128 | J. Am. Chem. Soc. 2012, 134, 11807−11814

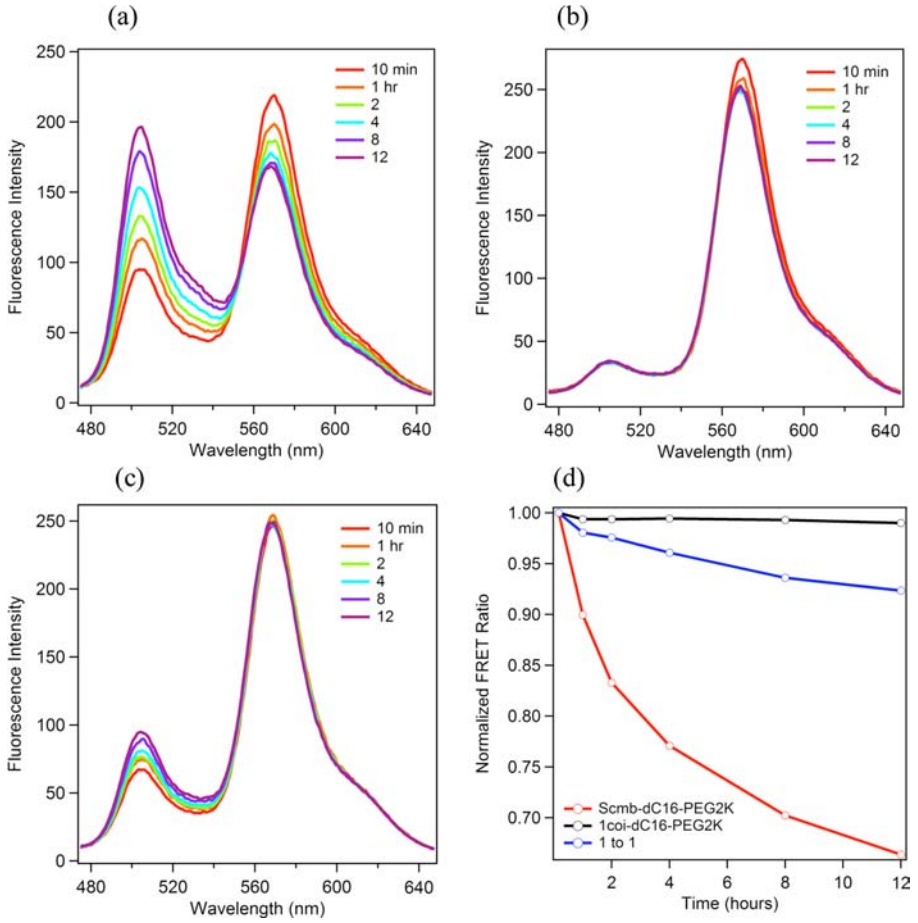

Figure 8. Stability of micelles with different headgroups by time-resolved FRET. (a) Scmb−dC16−PEG2K micelles encapsulating DiO and DiI FRET pair dyes. (b) 1coi−dC16−PEG2K micelles encapsulating DiO and DiI FRET pair dyes. (c) One-to-one hybrid micelles of 1coi−dC16−PEG2K and Scmb−dC16−PEG2K encapsulating DiO and DiI. (d) Plot of normalized FRET versus time.

critical to slow down the subunit exchange kinetics and the secondary protein structure is not sufficient. In fact, Figure 6b shows that a rigid helical peptide is even more effective in defining the radial position of conjugated polymer chains in a micelle than in a random coil. This leads to a higher repulsion among headgroups, thus providing stronger driving forces toward subunit desorption.

Micelle formation is driven by the hydrophobic interactions among alkyl tails, and the subunit exchange kinetics depends on the molecular packing of the hydrophobic tail. A crystalline hydrophobic core increases the energetic barrier for subunit exchange. Differential scanning calorimetry (DSC) was used to probe alkyl packing of C16 tails for the three micelles. All solutions were incubated at 20 °C for 16 h before the DSC measurements, where the micelle solution was heated from 5 to 85 °C at 1 °C/min. Scmb−dC16−PEG2K has a sharp endothermic peak with a melting temperature of 42 °C and a transition enthalpy of 40.4 ± 2.6 kJ/mol (Figure 7a); thus, conjugating PEG to the side chain of this random coil did not compromise the ordering of the alkyl chains. For Singlehelix−dC16−PEG2K, the melting temperature was reduced to ∼33 °C and the transition enthalpy is 40.1 ± 2.0 kJ/mol (Figure 7b). For 1coi−dC16−PEG2K, two broad peaks centered at 17 and 32 °C with a total transition enthalpy of 39.7 ± 4.2 kJ/mol were observed (Figure 7c), since the repulsion among the neighboring PEG chains leads to splaying of alkyl chains.[25] Even though the hydrophobic core was mainly disordered at 20 °C, 3-helix micelles exhibit much slower subunit exchange kinetics than that of micelles with a crystalline alkyl core. This, again, confirms that the corona layer of the micelle provides the driving forces to stabilize micelles.

The formation of 3-helical bundles also increases the molecular mass of the desorbed subunits and the overall hydrophobicity of the subunits by binding of six aliphatic chains together, as opposed to two in the case of Scmb−dC16−PEG2K and SingleHelix−dC16−PEG2K. Both may increase the energetic barriers for subunit exchange and slow down the subunit exchange kinetics. However, based on previous work on amphiphilic block copolymers, we do not expect these changes to be the dominant factor of slow subunit exchange kinetics. In fact, for either case to be the main factor, it is required that the amphiphile desorbs as a trimeric subunit rather than a monomer. Since it is difficult to determine the oligomeric state of the desorbed amphiphile, we performed FRET experiments using mixtures of 1coi−dC16−PEG2K and Scmb−dC16−PEG2K, where Scmb−dC16−PEG2K can readily desorb as monomers. The stability of the hybrid micelles was monitored by FRET in the presence of bovine serum albumin (BSA), which is known as an amphiphile trap that accelerates subunit desorption.[26,50] The lipophilic FRET pair dyes, DiO (donor) and DiI (acceptor), were coencapsulated in micelles composed of a 1:1 molar ratio mixture of 1coi−dC16−PEG2K and Scmb−dC16−PEG2K. Micelle solutions of pure 1coi−dC16−PEG2K and Scmb−dC16−PEG2K were also prepared.

dx.doi.org/10.1021/ja3048128 | J. Am. Chem. Soc. 2012, 134, 11807−11814

For all three micelle solutions, due to the close proximity of the dye molecules, initially FRET turns on and the fluorescence spectra show a major fluorescence emission peak at 565 nm and a minor peak at 505 nm. If the cargo molecules leach out, FRET turns "off," resulting in a simultaneous increase of fluorescence intensity at 505 nm and a decrease at 565 nm. As shown in the time-dependent fluorescence spectra (Figure 8a), the emission maximum shifts from 565 to 505 nm for Scmb−dC16−PEG2K, indicating that the dye molecules were released to the medium, while the fluorescence intensity of 1coi−dC16−PEG2K at both 565 and 505 nm remains essentially unchanged (Figure 8b). These results are consistent with the kinetics studies shown in Figure 4 and 6a. Through coassembly with a 1:1 ratio, as shown in Figure 8c, the stability of the hybrid micelles was greatly enhanced as compared to that of pure single chain micelles composed of Scmb−dC16−PEG2K. The FRET ratio of $I_{565}/(I_{565} + I_{505})$ is used to estimate the efficiency of energy transfer and reflects the relative stability of micelles.[51−53] Figure 8d shows the normalized FRET ratio as a function of time. After 12 h of incubation in BSA, the FRET ratio is 0.66, 0.99, and 0.92 for single chain micelles, 3-helix micelles and the hybrids, respectively. The higher FRET ratio observed for the mixture micelle demonstrates that the kinetics of desorption of monomeric amphiphiles are greatly depressed in the presence of the 3-helix bundles. The presence of protein tertiary structure, i.e. 3-helix bundle formation in the amphiphile headgroup, increases the energetic barrier for monomeric amphiphile desorption.

In the amphiphile design, we hypothesize that the formation of 3-helix bundles essentially positions the directionality of the force exerted by the compressed PEG chains. PEG chains act as elastic springs to hold the neighboring subunits from desorption. Thus, the key to the stability of the micelles lies in the PEG chains anchored to the exterior of the helix bundle and their spatial arrangement. For 1coi-PEG2K, the radius of gyration of PEG is ∼1.2 nm, as determined by the small-angle X-ray scattering.[46] We are in the process of performing neutron scattering studies to quantify the PEG chain conformation upon micelle formation. For now, we derive this by estimating the volume occupied by each trimeric subunit. Using analytical ultracentrifugation (AUC), the aggregation number of each micelle was determined to be ∼45, i.e. ∼15 trimolecular subunits per micelle. We modeled the PEG chains in 1coi−dC16−PEG2K micelles as entropic springs and estimated a change in elastic energy of the PEG chains compressed in the micelle shell relative to their unperturbed state in the buffer solution. The elastic energy was estimated to be ∼10 kcal/mol using $U = 1/2\kappa x^2$, where x^2 is proportional to the difference in the mean square end-to-end distance between a PEG chain in the micelle and in its free state, and the effective spring constant, κ, is inversely proportional to the mean square unperturbed dimensions. The elastic energy can be manipulated by varying the PEG chain length and the site of conjugation. Future study will be focused on the quantitative measurement of PEG chain conformation by neutron scattering for amphiphiles with PEG2K and PEG5K as well as amiphiphiles with PEG at different positions. The systematic analysis will help better understand the role of entropic repulsion in micelle formation, stabilization, and disassembly. Overall, by controlling the radial and lateral positions of elastic energies stored in the PEG chains, these repulsive forces act synergistically to stabilize high-curvature nanostructures that would otherwise be impossible to obtain.

CONCLUSION

In summary, we systematically investigated a range of parameters governing the kinetic stability of micelles based on amphiphilic 3-helix bundle-forming peptide−polymer conjugates. Combining the results from both thermal stability and kinetics measurements, there is strong evidence that the molecular structure of the hydrophilic headgroup plays a more important role in controlling the micelle stability than the hydrophobic chains. The protein tertiary structures can position entropic repulsive interactions of polymer chains comprising the headgroups so as to stabilize individual micelles (called 3-helix micelles), slow down subunit exchange, and retard cargo leakage. Furthermore, the micelle stability can be manipulated through coassembly of amphiphilic subunits with different headgroups. Incorporation of the 3-helix bundle peptide−polymer conjugate in nonpeptidic micelles may be a promising strategy to generate stable amphiphilic micelles comprising a wide range of molecular building blocks (including lipids and BCPs) by means of directed entropic repulsion. Overall, with the identification of various parameters in controlling the dynamic stability of amphiphilic micelles, present studies provide useful guidelines to the design and synthesis of micelles that are promising to overcome some of the existing stability barriers for their applications as nanocarriers and nanoreactors.

ASSOCIATED CONTENT

Supporting Information

Peptide purification methods, structural characterization methods by CD, DSC, SEC, and fluorescence; structure characterization results by SAXS and TEM; CMC results by pyrene encapsulation method. This material is available free of charge via the Internet at http://pubs.acs.org.

AUTHOR INFORMATION

Corresponding Author

tingxu@berkeley.edu

Notes

The authors declare no competing financial interest.

ACKNOWLEDGMENTS

H.D. was supported by the Office of the Army, U.S. Department of Defense under Contract W91NF-09-1-0374. J.Y.S, N.D., Y.M, M.T., and T.X. were supported by the Office of Science, Office of Basic Energy Sciences, the U.S. Department of Energy under Contract DE-AC02-05CH11231. Use of the Advanced Light Source is supported by the Director, Office of Science, Office of Basic Energy Sciences, U.S. Department of Energy under Contract No. DE-AC02-05CH11231. Neutron scattering studies were carried out at Oak Ridge National Laboratory's High Flux Isotope Reactor sponsored by the Scientific User Facilities Division, Office of Basic Energy Sciences, U.S. Department of Energy. We thank Dr. Oleg Gang for scientific discussion on entropic repulsion and Dr. Reidar Lund for help on kinetics data fitting.

REFERENCES

(1) Shi, J.; Votruba, A. R.; Farokhzad, O. C.; Langer, R. *Nano Lett.* **2010**, *10*, 3223−3230.

(2) Kataoka, K.; Harada, A.; Nagasaki, Y. *Adv. Drug Delivery Rev.* **2001**, *47*, 113−131.

(3) MacKay, J. A.; Chen, M.; McDaniel, J. R.; Liu, W.; Simnick, A. J.; Chilkoti, A. *Nat. Mater.* **2009**, *8*, 993−999.
(4) Peters, D.; Kastantin, M.; Kotamraju, V. R.; Karmali, P. P.; Gujraty, K.; Tirrell, M.; Ruoslahti, E. *Proc. Natl. Acad. Sci. U.S.A.* **2009**, *106*, 9815−9819.
(5) Percec, V.; Wilson, D. A.; Leowanawat, P.; Wilson, C. J.; Hughes, A. D.; Kaucher, M. S.; Hammer, D. A.; Levine, D. H.; Kim, A. J.; Bates, F. S.; Davis, K. P.; Lodge, T. P.; Klein, M. L.; DeVane, R. H.; Aqad, E.; Rosen, B. M.; Argintaru, A. O.; Sienkowska, M. J.; Rissanen, K.; Nummelin, S.; Ropponen, J. *Science* **2010**, *328*, 1009−1014.
(6) Gref, R.; Minamitake, Y.; Peracchia, M. T.; Trubetskoy, V.; Torchilin, V.; Langer, R. *Science* **1994**, *263*, 1600−1603.
(7) Holder, S. J.; Sommerdijk, N. A. J. M. *Polym. Chem.* **2011**, *2*, 1018−1028.
(8) Elsabahy, M.; Wooley, K. L. *Chem. Soc. Rev.* **2012**, *41*, 2545−2561.
(9) Rösler, A.; Vandermeulen, G. W. M.; Klok, H.-A. *Adv. Drug Delivery Rev.* **2001**, *53*, 95−108.
(10) Cabral, H.; Matsumoto, Y.; Mizuno, K.; Chen, Q.; Murakami, M.; Kimura, M.; Terada, Y.; Kano, M. R.; Miyazono, K.; Uesaka, M.; Nishiyama, N.; Kataoka, K. *Nat. Nanotechnol.* **2011**, *6*, 815−823.
(11) Dong, H.; Dube, N.; Shu, J. Y.; Seo, J. W.; Mahakian, L. M.; Ferrara, K. W.; Xu, T. *ACS Nano* **2012**, *6*, 5320−5329.
(12) Liu, Y.; Wang, Y.; Wang, Y.; Lu, J.; Piñón, V.; Weck, M. *J. Am. Chem. Soc.* **2011**, *133*, 14260−14263.
(13) Klingelhöfer, S.; Heitz, W.; Greiner, A.; Oestreich, S.; Förster, S.; Antonietti, M. *J. Am. Chem. Soc.* **1997**, *119*, 10116−10120.
(14) Fan, H. Y. *Chem. Commun.* **2008**, 1383−1394.
(15) Lang, J.; Tondre, C.; Zana, R.; Bauer, R.; Hoffmann, H.; Ulbricht, W. *J. Phys. Chem.* **1975**, *79*, 276−283.
(16) Lessner, E.; Teubner, M.; Kahlweit, M. *J. Phys. Chem.* **1981**, *85*, 1529−1536.
(17) Gao, Z.; Eisenberg, A. *Macromolecules* **1993**, *26*, 7353−7360.
(18) Kwon, G. S.; Kataoka, K. *Adv. Drug Delivery Rev.* **1995**, *16*, 295−309.
(19) Lee, C. C.; MacKay, J. A.; Fréchet, J. M. J.; Szoka, F. C. *Nat. Biotechnol.* **2005**, *23*, 1517−1526.
(20) Lee, C. C.; Gillies, E. R.; Fox, M. E.; Guillaudeu, S. J.; Fréchet, J. M. J.; Dy, E. E.; Szoka, F. C. *Proc. Natl. Acad. Sci. U.S.A.* **2006**, *103*, 16649−16654.
(21) Fox, M. E.; Szoka, F. C.; Fréchet, J. M. J. *Acc. Chem. Res.* **2009**, *42*, 1141−1151.
(22) Diezi, T. A.; Bae, Y.; Kwon, G. S. *Mol. Pharm.* **2010**, *7*, 1355−1360.
(23) Lu, J.; Owen, S. C.; Shoichet, M. S. *Macromolecules* **2011**, *44*, 6002−6008.
(24) Zhao, X.; Poon, Z.; Engler, A. C.; Bonner, D. K.; Hammond, P. T. *Biomacromolecules* **2012**, *13*, 1315−1322.
(25) Kastantin, M.; Ananthanarayanan, B.; Karmali, P.; Ruoslahti, E.; Tirrell, M. *Langmuir* **2009**, *25*, 7279−7286.
(26) Kastantin, M.; Missirlis, D.; Black, M.; Ananthanarayanan, B.; Peters, D.; Tirrell, M. *J. Phys. Chem. B* **2010**, *114*, 12632−12640.
(27) Aniansson, E. A. G.; Wall, S. N. *J. Phys. Chem.* **1974**, *78*, 1024−1030.
(28) Aniansson, E. A. G.; Wall, S. N.; Almgren, M.; Hoffmann, H.; Kielmann, I.; Ulbricht, W.; Zana, R.; Lang, J.; Tondre, C. *J. Phys. Chem.* **1976**, *80*, 905−922.
(29) Nicolai, T.; Colombani, O.; Chassenieux, C. *Soft Matter* **2010**, *6*, 3111−3118.
(30) van Stam, J.; Creutz, S.; De Schryver, F. C.; Jerome, R. *Macromolecules* **2000**, *33*, 6388−6395.
(31) Won, Y.-Y.; Davis, H. T.; Bates, F. S. *Macromolecules* **2003**, *36*, 953−955.
(32) Lund, R.; Willner, L.; Richter, D.; Dormidontova, E. E. *Macromolecules* **2006**, *39*, 4566−4575.
(33) Zinn, T.; Willner, L.; Lund, R.; Pipich, V.; Richter, D. *Soft Matter* **2012**, *8*, 623−626.
(34) Joralemon, M. J.; O'Reilly, R. K.; Hawker, C. J.; Wooley, K. L. *J. Am. Chem. Soc.* **2005**, *127*, 16892−16899.
(35) Sun, X.; Rossin, R.; Turner, J. L.; Becker, M. L.; Joralemon, M. J.; Welch, M. J.; Wooley, K. L. *Biomacromolecules* **2005**, *6*, 2541−2554.
(36) Zhang, Q.; Remsen, E. E.; Wooley, K. L. *J. Am. Chem. Soc.* **2000**, *122*, 3642−3651.
(37) Samarajeewa, S.; Shrestha, R.; Li, Y.; Wooley, K. L. *J. Am. Chem. Soc.* **2011**, *134*, 1235−1242.
(38) Kellermann, M.; Bauer, W.; Hirsch, A.; Schade, B.; Ludwig, K.; Bottcher, C. *Angew. Chem., Int. Ed.* **2004**, *43*, 2959−2962.
(39) Israelachvili, J. N. *Intermolecular and Surface Forces: With Applications to Colloidal and Biological Systems*, 2nd ed.; Academic Press: Amsterdam, 1992.
(40) Israelachvili, J. N.; Wennerstrom, H. *J. Phys. Chem.* **1992**, *96*, 520−531.
(41) Sheiko, S. S.; Sun, F. C.; Randall, A.; Shirvanyants, D.; Rubinstein, M.; Lee, H.-i.; Matyjaszewski, K. *Nature* **2006**, *440*, 191−194.
(42) Kegel, W. K.; van der Schoot, P. *Biophys. J.* **2004**, *86*, 3905−3913.
(43) Siber, A.; Podgornik, R. *Phys. Rev. E* **2007**, *76*, 061906.
(44) van der Schoot, P.; Zandi, R. *Phys. Biol.* **2007**, *4*, 296−304.
(45) Gillies, E. R.; Dy, E.; Fréchet, J. M. J.; Szoka, F. C. *Mol. Pharmaceutics* **2005**, *2*, 129−138.
(46) Shu, J. Y.; Lund, R.; Xu, T. *Biomacromolecules* **2012**, *13*, 1945−1955.
(47) Ogihara, N. L.; Weiss, M. S.; Degrado, W. F. *Protein Sci.* **1997**, *6*, 80−88.
(48) Shu, J. Y.; Tan, C.; DeGrado, W. F.; Xu, T. *Biomacromolecules* **2008**, *9*, 2111−2117.
(49) Wang, Y.; Kausch, C. M.; Chun, M.; Quirk, R. P.; Mattice, W. L. *Macromolecules* **1995**, *28*, 904−911.
(50) Missirlis, D.; Khant, H.; Tirrell, M. *Biochemistry* **2009**, *48*, 3304−3314.
(51) Chen, H.; Kim, S.; He, W.; Wang, H.; Low, P. S.; Park, K.; Cheng, J. X. *Langmuir* **2008**, *24*, 5213−5217.
(52) Chen, H. T.; Kim, S. W.; Li, L.; Wang, S. Y.; Park, K.; Cheng, J. X. *Proc. Natl. Acad. Sci. U. S. A.* **2008**, *105*, 6596−6601.
(53) Jiwpanich, S.; Ryu, J.-H.; Bickerton, S.; Thayumanavan, S. *J. Am. Chem. Soc.* **2010**, *132*, 10683−10685.